Structural and optical properties of DNA layers covalently attached to diamond surfaces

Non Peer-reviewed author version

Structural and optical properties of DNA layers covalently attached to diamond surfaces

Sylvia Wenmackers[†,‡], Simona D. Pop[§], Katy Roodenko[§], Veronique Vermeeren[||,‡], Oliver A. Williams[†,+], Michael Daenen[†], Olivier Douhéret[†,+], Jan D'Haen[†,+], An Hardy[%,#], Marlies K. Van Bael[%,+], Karsten Hinrichs[§], Christoph Cobet[§], Martin vandeVen[||,‡], Marcel Ameloot[||,‡], Ken Haenen[†,+], Luc Michiels[||,‡], Norbert Esser[§], and Patrick Wagner[*,†,‡]

Hasselt University, Institute for Materials Research, Wetenschapspark 1, B-3590 Diepenbeek, Belgium, IMEC vzw, Division IMOMEC, Wetenschapspark 1, B-3590 Diepenbeek, Belgium, Hasselt University, Biomedical Research Institute, Agoralaan Building A, B-3590 Diepenbeek, Belgium, and Institute for Analytical Sciences, Department Berlin, Albert-Einstein-Straße 9, D-12489 Berlin, Germany.

Label-free detection of DNA molecules on chemically vapor-deposited diamond surfaces is achieved with spectroscopic ellipsometry in the infrared and vacuum ultra-violet range. This non-destructive method has the potential to yield information on the average orientation of single as well as double stranded DNA molecules, without restricting the strand length to the persistence length. The orientational analysis based on electronic excitations in combination with information from layer thicknesses, provides a deeper understanding of biological layers on diamond. The π-π* transition dipole moments, corresponding to a transition at 4.74 eV, originate from the individual bases. They are in a plane perpendicular to the DNA backbone with an associated n-π* transition at 4.47 eV. For 8-36 bases of single and double stranded DNA covalently attached to ultra-nanocrystalline diamond, the ratio between in- and out-of-plane components in the best fit simulations to the ellipsometric spectra yields an average tilt angle of the DNA backbone with respect to the surface plane ranging from 45° to 52°.

1

We comment on the physical meaning of the calculated tilt angles. Additional information is gathered from atomic force microscopy, fluorescence imaging, and wetting experiments. The results reported here are of value in understanding and optimizing the performance of the electronic read-out of a diamond-based label-free DNA hybridization sensor.

* Corresponding author. E-mail: patrick.wagner@uhasselt.be.

† Hasselt University, Material Physics - Institute for Materials Research.

‡ transnationale Universiteit Limburg, School for Life Sciences.

§ Institute for Analytical Sciences, Department Berlin.

‖ Hasselt University, Biomedical Research Institute.

+ IMEC vzw, Division IMOMEC.

% Hasselt University, Inorganic and Physical Chemistry – Institute for Materials Research.

\# XIOS Hogeschool Limburg, Department Industrial Sciences and Technology.

1. Introduction

A better understanding and characterization of layers of terminally attached deoxyribonucleic acid (DNA) molecules on a surface, DNA brushes, is important for improving genetic assays, where single stranded (ss) probe DNA is immobilized on a solid support and coupled (hybridized) to target ssDNA molecules from solution.

For electrical sensing, the substrate for attachment of the DNA probes should preferably be a metal or semiconductor. The material should be stable in solution and receptive for the covalent attachment of probe DNA. DNA brushes have successfully been prepared and extensively studied on materials such as silicon oxide[1] and gold.[2-8] In recent years, diamond obtained from chemical vapor deposition (CVD) gained interest with regard to biosensor applications. This stable, highly biocompatible material, can be applied in electrical sensing, thanks to its wide band gap and large electrochemical potential window.[9,10] Diamond surfaces range from single crystalline to ultra-nanocrystalline films,[11] and from undoped to (heavily) boron doped. Its surface has been functionalized successfully with various bio-molecules: DNA,[12-15] as well as immunoglobulins G and M (IgG and IgM),[16] and enzymes such as catalase,[17] urease and glucose oxidase,[18] as well as horse radish peroxidase.[19] DNA sensors for *in vitro* use only require a biocompatible top-layer, to which the probe DNA is anchored and where interaction with target DNA samples takes place. Diamond-coated silicon wafers are a good starting material, as they are easier to produce and cheaper than an all-diamond biosensor. Ultra-nanocrystalline diamond (UNCD®) coated silicon was indeed found to be a very stable platform for DNA.[12] In the current study, we will therefore focus on DNA layers grafted on nanocrystalline (NCD) and UNCD coated silicon.

Important parameters for good sensor functioning (hybridization) are the density and the orientation of the DNA molecules in the sensing layer. Molecular dynamics simulations of DNA molecules, based on classical worm-like chain (WLC) theory and adaptations thereof,[20,21] are in good agreement with recent experimental findings, such as cyclization studies,[12,22] bending force measurements based on magnetic tweezers and single-molecule fluorescence microscopy,[23] as well as AFM studies of DNA layers lying flat on mica.[24] However, it is not straightforward to predict, starting from these models for

the mechanical properties of DNA, the behavior of surface-bound DNA molecules. In DNA brushes, the density of the layer will most probably influence the orientation of the molecules. Therefore, we will first distinguish between 'dilute' and 'dense' DNA layers.

We will call the layer 'dilute' when the DNA spacing is comparable to or larger than the stretched-out length of the molecules, which implies that they do not interact substantially. The orientation of DNA in low density layers on gold substrates has been studied theoretically,[25] as well as experimentally.[26-29] One approach is to monitor the interfacial fluorescence quenching, which increases when the fluorescence dye at the distal end of DNA is brought closer to a gold substrate, while the gold electrode is biased to alternately positive and negative potentials.[26] Also atomic force microscopy (AFM) and scanning tunneling microscopy (STM) are applied to dilute,[27-29] as well as 'dense' DNA layers on gold.[2,3] When the DNA is in a dense layer, the molecules do interact, and the conformation and orientation of the molecules can become strongly affected by these interactions. These studies estimate the average tilt angles from the plane of the surface for DNA molecules on gold to be in the range of 45° to 60°. In a cyclic voltammetry study, using a ferrocene label at the distal end of DNA on gold electrodes, it was found that the DNA molecules can bend as well as rotate under applied electric fields.[5] The previously mentioned range for the average tilt angle of double stranded (ds) DNA molecules could be narrowed to 55° to 60°. In recent literature, the process steps of covering diamond with dense DNA layers have been validated using a variety of techniques, including X-ray photoelectron spectroscopy (XPS),[12,30,31] AFM,[14,32-34] ultraviolet photoelectron spectroscopy (UPS),[30] electrochemical impedance spectroscopy (EIS),[35-37] enzyme linked immunosorbent assays (ELISA),[31] amplification by polymerase chain reaction (PCR) followed by gel electrophoresis,[13] and fluorescence microscopy (FM).[12-14,31] Of this list, only the tapping mode (or intermittent-contact mode) AFM studies[14,32-34] were specifically aimed at clarifying the orientation of DNA molecules in dense layers. Based on the measurement of the DNA layer thickness, Rezek and Nebel report average tilt angles for 16 bp dsDNA on single crystalline diamond in the range of 30° to 37° with respect to the surface[14,34].

This estimation applies only to the analysis of short dsDNA, since it assumes that the molecules in the layer are straight.

In this work, the orientation of dense DNA molecules on CVD diamond is investigated. We use spectroscopic ellipsometry (SE) – both in infrared (IR) and ultra-violet (UV) – as a complementary technique to AFM. The SE approach allows the evaluation of layer thicknesses as well as average tilt angles, with the advantage of being applicable to both short and long DNA, and for both ds and ssDNA. SE is a useful characterization method for polymer brushes in general.[38] The samples in the current study consist of DNA end-grafted on NCD and UNCD surfaces. Functionalization is done by a two-step protocol, involving the photo-attachment of fatty acids to form a linker layer, followed by the covalent DNA attachment using a zero-length crosslinker, as reported in detail previously,[13] and confirmed later on.[15,39] To check whether the DNA forms a homogeneous layer we apply FM, as well as AFM for information on smaller scales. Based on the observation of vibrational bands, IR SE enables a direct, label-free proof of the DNA attachment, together with an estimation of the layer thickness. This technique has been used previously to determine the average tilt angle in guanine films on silicon.[40] With UV SE, electronic excitations are monitored, the orientation can be deduced,[41] and ss and dsDNA can be distinguished, as was already observed for non-surface-bound DNA in the early sixties.[42,43] DNA molecules are particularly interesting to be studied with SE in the UV range, because they contain transition dipole moments oriented along two well-defined directions: in the plane of the bases and, perpendicular to this, along the backbone of the strands.[44,45] SE has already been applied to study films of single bases on silicon,[40,45] but to our knowledge this is the first report on its application to study the average tilt angle of integral DNA molecules on CVD diamond surfaces. Although the analysis of SE measurements is more straightforward for atomically flat substrates, the roughness of NCD and especially UNCD films is low and regular enough to correct for by introducing an additional layer in the optical model, with intermediate optical properties.

2. Materials and Methods

Diamond preparation. After mechanical seeding of a Si(100) substrate with diamond powder, NCD films thinner than 200 nm were deposited, using a plasma enhanced (PE) CVD reactor "ASTeX® AX6550" from Seki Technotron Corp. (Tokyo, Japan) equipped with a 2.45 GHz microwave generator set at 3000 W, and applying 485 sccm H_2 (standard cubic centimeter per minute), 15 sccm CH_4, 40 Torr (= 5.3 kPa), 730°C for 80 min.[11] Typically, the NCD thickness decreases radially from the centre of the wafer, while UNCD shows a more homogeneous thickness throughout the wafer. Because thickness variations cause the background signal in SE to differ from place to place, also a 2 μm thick film of UNCD on a Si wafer, 'AQUA 25', deposited by Advanced Diamond Technologies (Romeoville, IL USA), was purchased through GoodFellow (Cambridge, UK).

The NCD and UNCD wafers were divided into 1 cm² squares and cleaned for 30 minutes in an oxidizing mixture of boiling sulfuric acid (H_2SO_4 98-100% pure, VWR International, Zaventem, Belgium) and potassium nitrate (KNO_3, ≥ 99%, Merck, Leuven, Belgium). This procedure was followed by thoroughly washing in distilled, ultra-pure water (18.2 MΩ.cm, obtained by filtering distilled water through an "Arium® 611 system", Sartorius, Göttingen, Germany): the water was changed six times, alternately heated and put in an ultrasonic cleaner ("Branson 1510", Branson, Danbury, UK). Afterwards, the samples were dried under a flow of nitrogen gas. The final H-termination was performed in a plasma at 700°C during 1 minute at 3000 W, 35 Torr (= 4.7 kPa) with 1000 sccm H_2.

Silicon preparation. For an ellipsometry reference experiment, three 1.5×1.5 cm² pieces of n-type Si(100) were H-terminated by the following three step treatment.[46-49] Firstly the samples were dipped in a mixture of H_2SO_4 (95%; Merck) and H_2O_2 (35%; Acros Organics) in a 4:1 volume ratio, secondly in a mixture of H_2O, H_2O_2 and NH_3 (32%; Merck) in 5:1:1 volume ratios, and thirdly in 5% HF (VWR International). Afterwards, the samples were rinsed in ultra-pure water and blown dry under nitrogen. The successful H-termination was evidenced by measurement of a grazing angle attenuated total reflection Fourier-transform IR (GATR-FTIR) spectrum (resolution 4 cm^{-1}; GATR Harrick, FTIR Bruker Vertex, Brussels, Belgium): peaks at 2137, 2114 and 2089 cm^{-1} were prominent, which are

attributed to the presence of SiH_3, SiH_2 and SiH respectively.[49] The H-terminated Si samples were put under the protective atmosphere of a nitrogen filled glovebox, after a short transportation time (~minutes) in air.

Diamond and silicon functionalization. Part of the H-terminated NCD, UNCD and Si samples were used for further functionalization. The NCD samples have been prepared exactly as described in reference 13, while the UNCD sample have been treated with the optimized conditions of reference 39. (Details on the functionalization can be found in the Supporting Information 1, Diamond functionalization, Fig. S1 and Table S1.) 10-undecenoic acid (UA) (Merck) is reacted with the surface during 20h under 254 nm UV illumination. This photo-reaction results in a carboxyl-terminated surface. Subsequent covalent coupling of amino-modified dsDNA to the carboxyl-terminated surface was carried out using the zero-length crosslinker 1-ethyl-3-[3-dimethylaminopropyl]-carbodiimide (EDC) (Perbio Science, Erembodegem, Belgium). This was done in 2-[N-morpholino]-ethanesulphonic acid (MES) buffer (Perbio Science). Here, different lengths of DNA were used, both ss of 8 or 36 b and ds of 250 bp, all with an amino-group at the 5' side. Part of the samples covered with 36 b ssDNA probes were allowed to hybridize to its perfect complement (29 b). The 250 bp dsDNA sample was denatured in 0.1 M sodium hydroxide (NaOH; Merck) to obtain a layer of 250 b ssDNA. For an SE reference experiment, a H-terminated sample was prepared with a multilayer of adsorbed DNA, formed by drying of a droplet of 250 bp dsDNA in buffer solution on an NCD substrate. The name codes for the various diamond samples can be found in Table 1. The UA functionalization of two of the Si(100) samples was performed similar to the method optimized for diamond,[39] but with the UV illumination time limited to 3 h to prevent the formation of a polymerized UA layer. One of the UA-terminated Si samples was then functionalized with 250 bp dsDNA.

Table 1: Overview of NCD and UNCD samples.

Sample name	Type of diamond	Surface termination
"N1"	NCD	Oxidized
"N2"	NCD	H-terminated
"N3"*	NCD	UA-linker layer
"N4"*	NCD	Brush of 250 bp dsDNA
"N5"	NCD	Adsorbed layer of 250 bp dsDNA
"U1"	UNCD	Oxidized
"U2"	UNCD	H-terminated
"U3"	UNCD	UA-linker layer
"U4+"	UNCD	Brush of 8 b ssDNA
"U4-"	UNCD	UA-linker layer and 8 b ssDNA without EDC
"U5"	UNCD	UA-linker layer and 8 b ssDNA without EDC
"U6"	UNCD	Brush of 36 b ssDNA
"U7"	UNCD	Brush of 29 bp dsDNA

*: these samples have been treated as described in reference 13.

Characterization techniques. For a morphology study, atomic force microscopy (AFM) was performed in tapping mode with a Veeco Multimode microscope (Veeco Instruments, Santa Barbara, CA USA) equipped with the Nanoscope III controller extended with the Quadrex module (phase signal imaging); high spatial resolution measurements (sub 10 nm) were ensured by the use of etched Si tips attached at the extremity of a standard non-contact mode cantilever (Nanosensors, Neuchâtel, Switzerland).

Spectroscopic ellipsometry (SE) analyzes the changes in the polarization state of radiation reflected from a dry sample surface (Fig. 1). These changes can be described by the measured ellipsometric parameters, $\tan(\psi)$ and Δ. The ellipsometric parameter $\tan(\psi)$ represents the amplitude ratio of the complex reflection coefficients parallel (r_s) and perpendicularly (r_p) polarized with respect to the plane of incidence ($\tan(\psi) = |r_p/r_s|$), while Δ is the phase shift between them (Fig. 1).
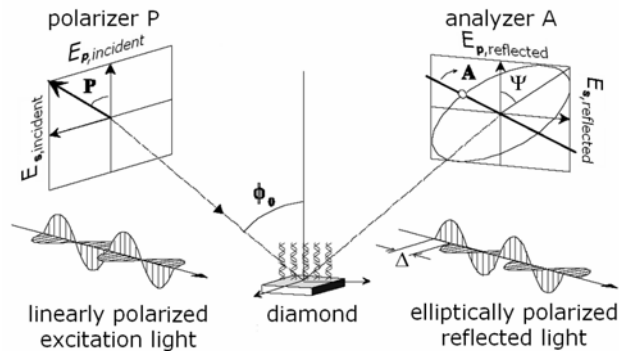
Figure 1: Schematic illustration of an ellipsometry measurement, defining the angles ϕ_0 and ψ, and the phase shift Δ.

IR ellipsometric measurements were performed on a photometric ellipsometer, attached to a Bruker 55 Fourier Transform spectrometer, as described in detail elsewhere.[50,51] The spectra were obtained with a resolution of 4 cm^{-1} using a Mercury Cadmium Telluride (MCT) detector, model "KV104-1", from Kolmar Technologies (Newburyport, MA, USA). Data analysis was performed as follows. The radiation propagation through the system consisting of Air/DNA/NCD was simulated in a 4×4 matrix formalism.[52] The simulation of the dielectric function was based on the isotropic Lorentz oscillator model.[51] The thickness of the thick DNA film on NCD (sample "N5") was first verified using a stylus profiler. Next, the oscillator strength and oscillator damping constants were fitted for the DNA layer on this sample using the above thickness and the vibrational frequencies υ_0 as reported for dsDNA at 25°C.[4] These oscillator values were used afterwards in the simulations of the spectra obtained for covalently bonded DNA on an NCD substrate (sample "N4"). For a cross-referenced analysis and calibration of the IR absorption bands, a well defined H-terminated Si(100) surface similarly modified with DNA layers was employed.

The UV ellipsometry measurements were performed under an incidence angle of ~68° to 69° at the Berliner Elektronenspeicherring-Gesellschaft für Synchrotronstrahlung (BESSY) synchrotron facility (Berlin, Germany) using a home-built rotating-analyzer ellipsometer operating in the 4.0–9.0 eV spectral range.[53-55]

3. Results

Scanning electron microscopy (SEM) images of the H-terminated NCD and UNCD surfaces can be found in Supporting Information 2 (Fig. S2 and S3). The functionalization steps have been validated using wetting studies (Supporting Information 3, Table S3) and fluorescence microscopy of labelled DNA (Supporting Information 4, Fig. S4-6), where the use of shadow masks during the photo-attachment of the linker layer is shown to yield clear patterns in the DNA layers (Fig. S7).

3.1. Morphology and roughness of NCD and UNCD surfaces. To obtain quantitative information on the roughness of the UNCD samples, tapping mode AFM experiments are performed on dry surfaces under ambient conditions.

3.1.1. NCD and UNCD surfaces with H- or UA-layer. The root mean square (RMS) roughness of the bare, H-terminated UNCD film (sample "U2") in Fig. 2 (a) is ~17 nm as determined with AFM on scales of (4 µm)² down to (1 µm)². The individual grains (sized between 3 to 50 nm) can be identified best in the phase image; in the normal height image larger clusters of grains can be seen. After photo-attachment of the UA linker molecule (sample "U3"), in Fig. 2 (b) the morphology and RMS roughness values do not significantly change. This is to be expected, since the length of a UA molecule is small (2 nm) compared to the surface roughness of the underlying UNCD film. No additional structures are found, indicating a homogeneous attachment of the UA layer to the surface, not limited to preferential sites (*e.g.* grain boundaries).
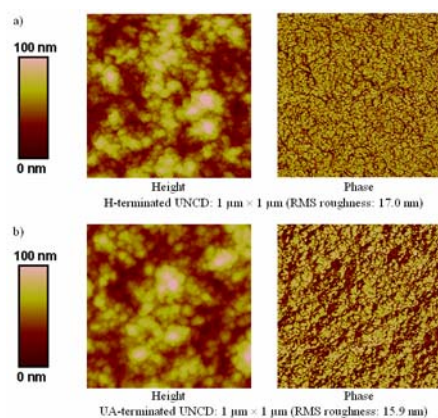

a)
100 nm

0 nm

Height | Phase
H-terminated UNCD: 1 µm × 1 µm (RMS roughness: 17.0 nm)

b)
100 nm

0 nm

Height | Phase
UA-terminated UNCD: 1 µm × 1 µm (RMS roughness: 15.9 nm)

Figure 2: 1 µm × 1 µm height and phase AFM images collected in tapping mode, in ambient conditions on a) H-terminated UNCD (sample "U2"), and on b) 10-undecenoic acid terminated UNCD (sample "U3").

3.1.2. NCD and UNCD surfaces with DNA-layer. Since the film roughness may have an impact on further ellipsometry results, we studied the change in morphology and RMS roughness of UNCD surfaces upon DNA attachment, by AFM in tapping mode. Although AFM measurements on DNA layers in buffer solutions are possible,[32] here the samples have been dried and measured in ambient conditions, because the ellipsometry measurements are (necessarily) performed on dry samples. The results are presented in Fig. 3. Throughout the measurements, the structures of the underlying UNCD stay dominant. To prevent denaturation, the samples with dsDNA are not rinsed in ultra-pure water, but dried with nitrogen directly from PBS buffer solution (containing NaCl, Na_3PO_4, and K_3PO_4). This causes some salt crystals, appearing as white spots in the height image (dark in the phase image) of Fig. 3 (c). In Fig. 3 (d) one such salt crystal is visible. However, the roughness is not significantly different for surfaces with H-termination only, or covered with an UA linker layer or with a layer of short ssDNA (8 b). For longer DNA (36 b), both in ss and ds form, the RMS roughness does decrease (Fig. 4). One can conjecture that here the biological top layer fills the dips between grains and grain clusters of the UNCD surface.
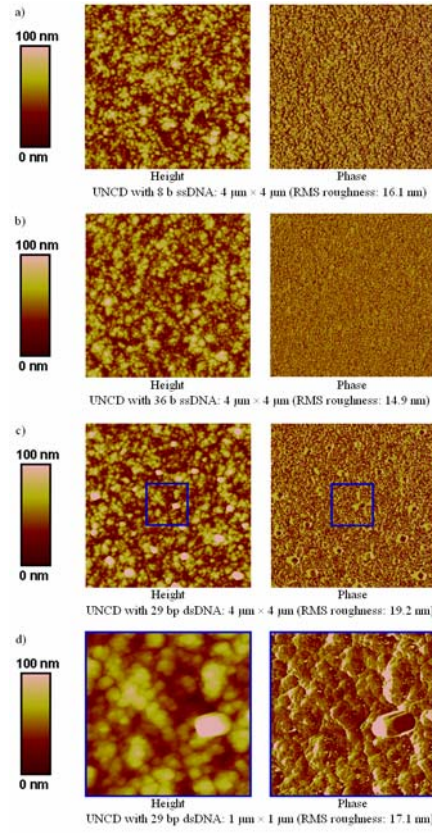
Figure 3: Height and phase AFM images in tapping mode, under ambient conditions on dry UNCD samples with varied surface terminations: a) UNCD with ssDNA of 8 b (sample "U5"), b) UNCD with ssDNA of 36 b (sample "U6"), and c) UNCD with dsDNA of 29 bp (on top of an A_7-ss-tail) (sample "U7"). d) More detailed scan of the square area indicated in part c).
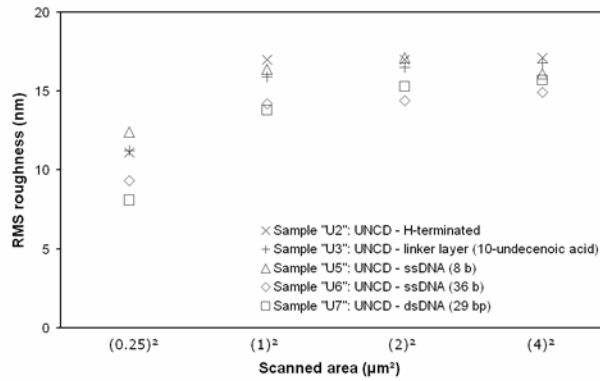

Figure 4: Comparison of RMS values of dry UNCD surfaces with different surface terminations as determined with tapping mode AFM on different scanning scales.

3.2. Label-free optical detection of DNA layers (in dry condition)

3.2.1. Average layer thickness of DNA layers on NCD. Ellipsometry in the IR range allows for a direct, label-free proof of the DNA immobilization on an NCD substrate. Fig. 5 shows typical spectra of DNA adsorbed or covalently attached to NCD and Si(100), in the region of the 'amide I' band, related to vibrations of amino and carbonyl groups.[4,56] All films show similar absorption properties, indicating that the DNA attachment was successful. Fig. 5 (c) also shows IR SE spectra for the UA-terminated Si(100) sample. The band around 1720 cm^{-1} is due to the carbonyl stretching vibrations of the carboxylic acid.[57] Upon DNA-attachment (Fig. 5 (d)), this band disappeared from the spectra of DNA on Si(100) samples, while the CH$_2$-related stretching vibrations of the hydrocarbon chains of the UA in the range between 2830-2980 cm^{-1} [57] remained unchanged. We did not observe similar bands on UA-terminated NCD substrates, probably due to a lower signal-to-noise ratio. The simulation of the measured results for DNA-terminated surfaces is shown in Fig. 5 by black solid lines. The simulated spectra were achieved using the isotropic Lorentz oscillator model and radiation propagation in a three layer Air/DNA/Substrate system, as described in detail in the "Materials and Methods" section. The determined thickness for the adsorbed 250 bp dsDNA layer on NCD (sample "N5") is $d = 200$ nm, and the high-frequency refractive index is $n_\infty = 1.51$. The oscillator parameters obtained from the simulations of the thick film data are then used to determine the thickness of the covalently-attached DNA layers on NCD (sample "N4") and Si(100) surfaces. Under the assumption that these films are isotropic, the calculations resulted in 40 nm thickness for 250 b ssDNA on NCD and 9 nm thickness for 250 bp dsDNA on Si(100) (with $n_\infty = 1.51$). The thickness of DNA on Si(100) was cross-checked with the ellipsometric measurements in the visible (VIS) spectral range. Estimated thickness accuracy is within 20% from the obtained thickness values, taking into account the results obtained from different methods and IR SE simulations on various samples. The high-frequency refractive index $n_\infty = 1.51 \pm 0.03$ as found by VIS ellipsometry and IR SE was in a good agreement with literature data.[58,59]

We would like to point out that the IR intensities reported in this work for layers of entire DNA molecules are in general smaller than those obtained for films of single DNA bases (*i.e.* adenine, thymine, guanine, and cytosine).[45] This decrease in intensity and frequency shifts upon base pairing has

13

also been observed by other authors.[57,60] However, additional studies are necessary in order to relate the IR intensities of the single DNA bases to those of DNA molecules.

The thickness as found for 250 b ssDNA covalently attached on NCD is less than the stretched-out length of the DNA, *i.e.* 150 nm. We give two possible explanations for this observation. First, the DNA strands are longer than the persistence length, the length scale over which dsDNA maintains its tangent orientation, *i.e.* ~2 nm,[61,62] so they are almost certainly not fully stretched on the NCD surface. For shorter DNA, there is a possibility of a tilt angle with respect to the diamond surface. Unfortunately, the complexity of the bands in the 'amide I' region does not allow for the determination of such a tilt angle, as was done in the case of pure guanine films using IR ellipsometry.[40] Therefore, we have investigated the band at 4.74 eV, with UV SE, as will be described now.
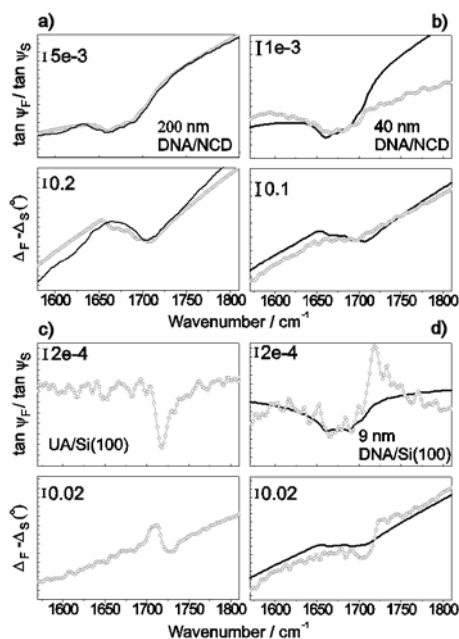

Figure 5: Referenced ellipsometric parameters tan(ψ) and Δ as obtained in IR SE measurements at 65° incidence angle. a) Adsorbed 250 bp dsDNA on NCD (sample "N5"); b) covalently attached 250 b ssDNA on NCD (sample "N4"); c) Si(100)-UA; d) Si(100)-UA-DNA. The grey dotted lines represent measured data referenced to a bare, H-terminated substrate; the simulations are presented as a black, solid line. Tan(ψ)$_S$ and Δ_S refer to the H-terminated NCD substrate, whereas tan(ψ)$_F$ and Δ_F refer to the sample with organic functionalisation. In (b) the difference in background between the measured data

and the simulation are due to differences between the H-terminated NCD reference sample and the NCD underlying the DNA film. In (d), the feature at about 1720 cm^{-1} arises from referencing to the UA-terminated Si(100) shown in (c), related to the C=O carbonyl group of the linker. The evaluated layer thicknesses are indicated on the plots. The high-frequency refractive index was n_{∞} = 1.51 in the calculations. In all calculations, substrates were simulated using the measured substrate optical constants, *i.e.* the refractive index n and the extinction coefficient k.

3.2.3. Average tilt angle of DNA molecules on NCD and UNCD. Besides IR SE, also ellipsometry in the vacuum ultra-violet (VUV) spectral range was applied, which reveals specific information on the electronic fingerprint of DNA molecules. The UV SE spectra of the thin, covalently attached DNA layer attached to an NCD substrate (sample "N4") are presented in Fig. 6 (a). The ellipsometric parameters tan(ψ) and Δ have been calculated using a three layer model (as explained under "Materials and Methods") assuming a DNA layer thickness of 40 nm and a high-frequency refractive index, n_{∞} = 1.51, as determined by IR SE. The optical response of the ssDNA layer was described by a sum of Lorentz functions. The obtained isotropic optical constants are displayed in Fig. 6 (b). The energy positions of the employed Lorentz functions are indicated by arrows. The typical π-π* electronic transition (representing an orbital change from bonding to anti-bonding) of the DNA molecule is observed at 4.74 eV (261 nm) in agreement with the values reported already in early literature.[44] Although it is well known that UV can damage DNA,[63-65] the presence of this non-shifted π-π* electronic transition suggests that UV dose is low enough during the UV SE measurement for the DNA layer to remain intact. This absorption band is assigned to the π-π* electronic transitions of the single DNA bases.[40,44] In the higher energy range the absorption structures are dominated by mixed π-π* and σ-σ* electronic transitions which belong to both single bases and sugar phosphate groups.[44]

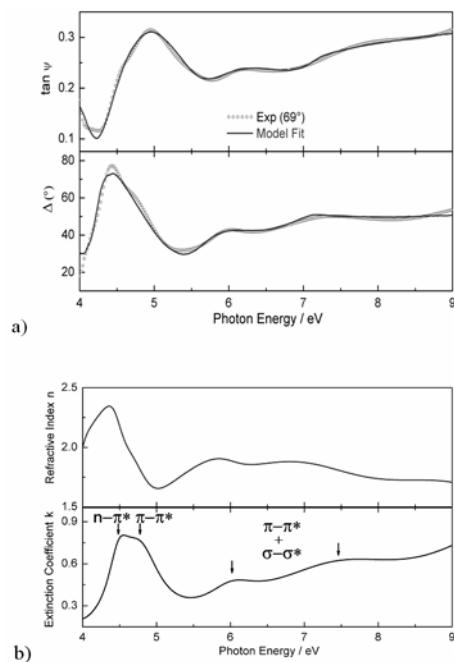**Figure 6**: Covalently attached monolayer of 250 b ssDNA on dry NCD (sample "N4"). a) Measured and calculated ellipsometric spectra tan(ψ) and Δ of this sample. b) Derived optical constants, refractive index (n) and extinction coefficient (k). The assignment of the main electronic transitions of DNA molecules is indicated by arrows.

The steep increase in the absorption above 7 eV is mainly due to σ-σ* transitions of the phosphate groups.[44] The lowest electronic transition at 4.47 eV (277 nm) assigned as an n-π* transition is a fingerprint for the molecular orientation, but also discriminates between the ss and ds conformation of DNA molecules.[42,43] The molecular orientation can be deduced, knowing that the n-π* transition dipole moment is directed along the DNA backbone, which is perpendicular to the π-π* transition dipole moments of the individual bases, as is schematically depicted in Fig. 7. On sample "N4", the optical response of the 250 b ssDNA layer is isotropic, meaning that the DNA molecules are mostly randomly distributed on the NCD substrate. This was to be expected, since ssDNA is a highly flexible polymer with a persistence length of only ~2 nm,[61,62] much shorter than its stretched-out length of 150 nm.
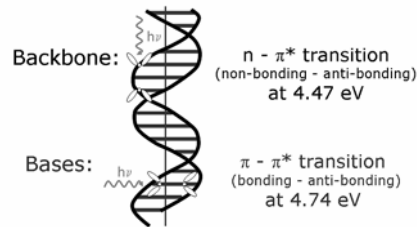
Figure 7: Schematic representation of the transitions at 4.47 and 4.74 eV in dsDNA.

Further UV SE experiments have been conducted for diamond surfaces terminated with a dense layer of short covalently attached DNA molecules, where a preferential orientation is expected. We have opted for DNA-functionalized UNCD rather than NCD, since the higher intrinsic roughness of NCD and its radially varying thickness was occasionally found to interfere with the signal coming from the DNA top layer. The dose of UV illumination during the UV SE experiments was low enough not to degrade the DNA films. This has been checked by measuring the same spot of the same sample twice, which resulted in exactly the same spectrum.

Fig. 8 shows the measured ellipsometric spectra of an H-terminated UNCD substrate (sample "U2"), ssDNA (36 b) (sample "U6"), and dsDNA (29 bp, connected to an A_7-ss-tail) (sample "U7") layers on UNCD substrates. These reveal notable differences between the ss and dsDNA layers, especially in the high energy range. The optical response of the DNA layers on UNCD substrate has been described by a uniaxial anisotropic layer model consisting of two sets of Lorentz functions corresponding to the in-plane (xy) and out-of-plane (z) directions of the film, as has been employed previously for pure guanine films on silicon.[40,45] The optical response of the measured substrate has been used in the ellipsometric modeling. The model has the advantage of taking into account the roughness of the UNCD substrate before introduction of DNA (see AFM result in Fig. 2 (b), where the RMS roughness of the UA-terminated surface is found to be ~16 nm) by employing the effective dielectric function, while having the disadvantage that the microscopic curvature of the surface is not included explicitly. Therefore, the extracted average molecular orientation of the DNA molecules must be interpreted carefully. The calculated spectra tan(ψ) and Δ of ss and dsDNA layers on UNCD substrate are given in Fig. 8 by solid

17

lines. The film thickness of the 36 b ssDNA (with a stretched-out length of 22 nm) layer is about 7.6 nm with a surface roughness of 0.7 nm, while the layer of 29 bp dsDNA (on top of an A_7-ss-tail, giving a total stretched-out length of 14 nm) amounts to a film thickness of about 10.8 nm and a surface roughness of 1.7 nm.
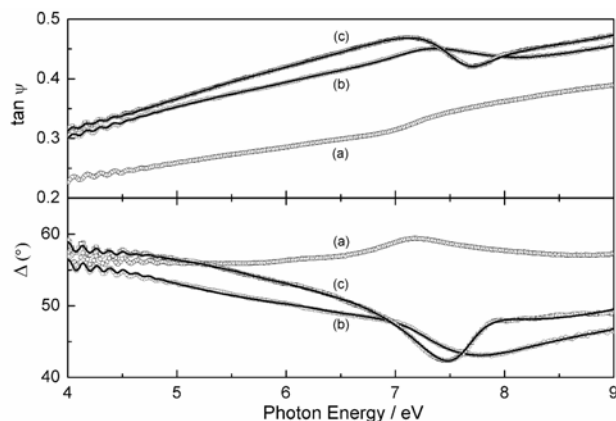

Figure 8: UV ellipsometric spectra of a) H- terminated UNCD ("U2"), b) 36 b ssDNA layer on UNCD ("U6"), and c) 29 bp dsDNA (connected to an A_7-ss-tail) layer on UNCD ("U7"). The experimental data are represented by open symbols. The calculated ellipsometric spectra using a uniaxial model are given by solid lines.

For the 8 b ssDNA layer (sample "U5"), the film thickness is 3.7 nm and the additional surface roughness is 0.3 nm, while the stretched-out length of 8 b ssDNA is 5 nm. Knowing the precise direction of the transition dipole moment corresponding to the lowest π-π^* electronic transitions of single DNA bases from 4.7 eV, the average molecular orientation of the DNA molecules can in principle be extracted.[39-41] Thus, the bases of the 8 b ssDNA molecules adopt an average tilt angle of 45° with respect to the substrate plane, while the bases of the longer 36 b ssDNA molecules seem to be tilted on average by 41°, implying that the backbones of the strands are tilted at 45° and 49° respectively (Fig. 9). The dsDNA molecules orient on average on the surface under a tilt angle of 52° with respect to the surface plane, a higher tilt angle than the ones obtained for ssDNA molecules of the same length. These averages are taken over the size of the VUV excitation spot on the surface, ~0.05 mm², and do not exclude the possibility of micro-domains showing different molecular orientations. The

18

tilt angle is a parameter used to describe the optical anisotropy of the layers. Its physical interpretation will be addressed in detail in the "Discussion and Conclusion" section.
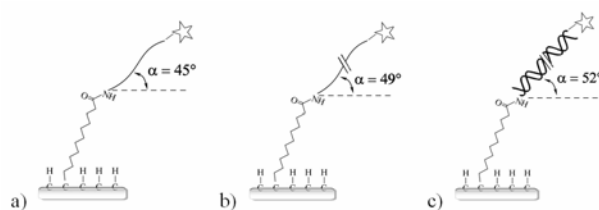

Figure 9: Average tilt angles of DNA molecules on UNCD as calculated from UV SE: a) 8 b ssDNA, b) 36 b ssDNA, and c) 29 bp dsDNA (connected to an A_7-ss-tail). (Not drawn to scale.)

4. Discussion and Conclusions

In the experimental work we have presented here, we have studied dense layers of ss and dsDNA molecules attached to NCD and UNCD diamond surfaces, because DNA brushes on a semi-conducting, bio-compatible material are of great relevance for DNA sensors. Label-free detection of DNA on NCD and UNCD diamond surfaces has recently been demonstrated with impedance measurements,[35-37] and now with spectroscopic ellipsometry. Our main goal was to determine the average orientation of the attached DNA molecules. Such a study has been reported[33] using tapping mode AFM of DNA layers on single-crystalline diamond surfaces.

To monitor the morphology and roughness of the dry samples, we have applied tapping mode AFM measurements under ambient conditions. From the AFM images of dry DNA films, we conclude that the DNA forms a dense layer on UNCD, following the underlying UNCD structure (Fig. 3). We have observed that the surface roughness of UNCD is not significantly altered upon the introduction of the 2 nm long linker molecule, nor after the attachment of short ssDNA of 8 bases, while it slightly decreases upon the introduction of DNA consisting of 36 bases, both for the ss and ds situation (Fig. 4). This decrease in RMS roughness, suggests that the biological top layer fills the dips between grains and grain clusters of the UNCD surface. We would like to point out that this result for dense DNA-layers on UNCD is the opposite to what has been reported for AFM measurements in buffer after the introduction of dilute end-tethered DNA layers on flat gold surfaces: starting from a very flat surface, the presence of low concentrations of 20 b ssDNA increases the surface roughness, and hybridization does this even more,[6,66] whereas on our samples the organic layer mostly follows the underlying structure, smoothing out the edges. Of course, the RMS roughness values also depend on the scanned area (Fig. 4), *i.e.* the smallest scan of (0.25 μm)² gives the smallest roughness estimation.

The signature of DNA in IR SE was first recorded on a sample containing a multilayer of 250 bp dsDNA (0.2 μm thick); the same spectral features could be identified for a monolayer of 250 b ssDNA on NCD, where the DNA layer thickness was found to be 40 nm, or about one fourth of the stretched-out length of the molecules. Although this may suggest a tilted orientation of the DNA molecules,

coiling up seems more likely for highly flexible single strands much longer than their persistence length (~2 nm).[62,67] However, the orientation could not be deduced based on IR SE alone, due to the complexity of the bands in the 'amide I' region.

Therefore, a more detailed analysis has been carried out in the VUV spectral range. The molecular orientation can be clarified from the analysis of the absorption at 4.74 eV, due to the π-π* transition dipole moments of the individual bases. The electronic n-π* transition at 4.47 eV is also a fingerprint for the molecular orientation, and discriminates between the ss and ds conformation of DNA molecules.[42,43] It was verified that the amount of UV illumination during the measurements did not influence above results by unintended degradation of the DNA layers. For the thin layer of 250 b ssDNA on NCD no preferential orientation is to be expected, and indeed the DNA layer is found to be isotropic: the DNA molecules are randomly distributed over the NCD substrate. For covalently attached layers of shorter DNA on UNCD, some directional preference is likely,[33] and we confirm the layers to be optically anisotropic. The mean square error in the best-fit simulation was a factor 3 better for anistropic conditions in comparison to an isotropic fit. For the best fit simulation of the 3.7 nm thick 8 b ssDNA layer we find an average tilt angle of 45° with respect to the surface plane, for the 7.6 nm thick 36 b ssDNA layer an angle of 49°, and for the 10.8 nm thick 29 bp dsDNA (connected to an A_7-ss-tail) layer an angle of 52°. The physical interpretation of the average tilt angle parameter deserves further explanation: it is related to intra- and intermolecular effects, as well as interactions of the DNA molecules with the substrate. It is the intermolecular level, describing the organisation of the DNA strands in the brush, that we are most interested in, but we will first address the two other factors.

Firstly, the orientation of the molecules (*i.e.* either the average direction of the single backbone, or the axis direction of the double helix) has not been probed directly, only the (average) orientation of the individual bases. The direction perpendicular to the plane of the bases is considered as that of the DNA-molecule. In case of dsDNA, the two strands are not oriented along the axis of the double helix, but make turns around it. Still, the orientation of the transition dipole moment along the bases averages out

to the plane perpendicular to the central axis of the double helix. Therefore, the tilt angle obtained for dsDNA can safely be interpreted as the average orientation of the double helices.

Secondly, although the microscopic form of the surface was not included explicitly, it has been taken into account implicitly, by using the effective dielectric function, based on a UV SE measurement of the bare, H-terminated substrate. As can be seen from the AFM image in Fig. 2 (b), the initial UNCD surface with the UA-linker layer has an RMS roughness of ~16 nm. The DNA layers are found to be only 4 to 11 nm thick, *i.e.* lower than the surface roughness. The reported tilt angles thus represent the average DNA orientation towards the plane of the surface on a macroscopic scale. Yet they are caused by the local molecular organisation in the DNA film, as well as the substrate topology. Since in this paper we have shown that our two-step attachment protocol also works on Si(100), we plan additional reference measurements on atomically flat silicon surfaces and single-crystalline diamond to clarify the influence of substrate roughness more precisely. Moreover, the results do not exclude the possibility of micro-domains: they are average values, taken over the size of the UV excitation spot on the surface. The lateral variation on the values will be investigated by SE mapping in later studies.

Because the results reported here have been obtained for dense DNA-brushes, we are confident that the topology is in any case not the only factor responsible for the observed tilt angles. In this case the intermolecular interactions are considerable and will prevent the DNA strands from perfectly following the substrate – as would be the case for molecules in a dilute, adsorbed layer. So now we come to the influence of these intermolecular interactions on the reported tilt angles. Although we have found higher angles for samples with more biological material (*i.e.* for longer DNA and after hybridization), we will not consider these angles as significantly different *per se*. Yet, the fact that for different samples, average tilt angle values of the same order are found, gives confidence in the analysis. Even if the average angles can be considered equal, the underlying distribution might differ: *e.g.* for ssDNA and dsDNA of the same length the higher flexibility of the ss molecules can result in a larger spread of the orientation.[2]

The values we find are comparable to those reported for 15 bp dsDNA on gold surfaces, for which an average tilt angle of 55°-60° with respect to the surface plane is found.[5] Yet, in literature on AFM on diamond, smaller tilt angles are reported: 30°-37° with respect to the surface for 16 bp dsDNA on top of a 15 b ssDNA-tail for dense layers on single crystalline diamond.[14,32-34] An important remark is that the AFM measurements on diamond[14,32-34] have been performed in buffer solutions, whereas our IR SE measurements were performed under ambient conditions, and UV SE measurements were performed in vacuum, requiring dry films. This may well influence the orientation of the molecules in the DNA layer, due to Debye screening and depending on the ionic strength of the buffer solutions. The higher roughness of UNCD as compared to single-crystalline diamond surfaces, the different linkers and the DNA density may also play a role. Another difference is that the signal of micro-domains in the DNA layer with a different orientation (if any) will be averaged out during the SE measurements (over the area of the beam), while in principle they could be probed by AFM individually. For DNA molecules in buffer solution there will be movement due to Brownian motion, but under vacuum conditions necessary for the UV SE measurements, no additional temporal averaging occurs.

An advantage of SE, however, is the more direct way of observing the orientation as reflected in the anisotropy of the optical properties, instead of an indirect conclusion based on measured layer thicknesses, the assumption that the DNA behaves as a stiff rod (which is only applicable to dsDNA shorter than the persistence length), and basic trigonometry. For three samples ("U4+", "U6", and "U7"), the average tilt angles (θ_{tilt}) for DNA on UNCD have been evaluated with UV SE from the direct detection of the orientation of the transient dipole moments of the bases. For these three samples, also the layer thicknesses are known from ellipsometry. Molecular tilt angles are commonly estimated from the way the observed layer thickness (obtained from AFM or ellipsometry) compares to the stretched-out length of the molecules in the layer.[2,33] The layer thickness obtained from vacuum UV SE is denoted T, and assuming that the molecules in the layer can tilt on the surface but not bend (like a stiff rod) having a certain stretched-out length, L, simple geometry shows that their tilt angle equals Arcsin(T/L). For sample "U7", covered with rigid dsDNA-fragments, excellent correspondence between the

geometrically based and experimentally obtained tilt angle is obtained: 50° and 52°, respectively. (A discussion including the other samples can be found in Supplementary Information 5, Table S3.)

We conclude that the modeling of DNA-brushes on a rough surface is far from trivial, and a direct way of observing the orientation is in most cases preferable to calculations based on layer thicknesses, obtained from *e.g.* non-spectroscopic ellipsometry, or nano-shaving AFM experiments.[14,32-34] Yet, for the DNA layer with the highest molecular stiffness (on sample "U7"), where thus the use of Arcsin(T/L) as a measure for the molecular tilt angle is best applicable, the average tilt angle obtained from the analysis of electronic excitations with UV SE is in excellent agreement with this geometrically estimated value. With the method presented in this paper, the orientation can be investigated directly, for ds as well as ssDNA, without restricting the strand length to the persistence length. To discriminate between the influence of the substrate topology and the intermolecular interactions on the tilt angle, additional reference measurements on atomically flat substrates are required. As such, the calculation of tilt angles with VUV SE has the potential of having a wider range of applicability than the aforementioned techniques, while combining it with the information on layer thicknesses gives us a richer understanding of biological layers on CVD diamond.

As a final point, we would like to comment on how the reported results with DNA brushes covalently attached to CVD diamond surfaces can be applied to improve the performance of diamond-based DNA sensors. Although additional experiments with mapping SE are required to evaluate lateral variation of the reported average tilt angles for 3 types of DNA layers, the influence of the substrate topology, and to determine whether the observed difference are to be considered significantly different, we have presented a technique that is in principle capable to detect such differences. Since best sensor performance is expected for more upright orientations of the probe ssDNA, combined with a moderate density not hindering hybridization, using this method, fabrication methods resulting in advantageous probe ssDNA layer properties can be identified and selected for use in DNA sensors. As an example, consider the method to deposit the layer of probe ssDNA: taking into account the differences in persistence length for ss and dsDNA, one can speculate that a layer of ssDNA obtained by

24

immobilization of dsDNA followed by denaturation (Supporting Information, Fig. S1 (c1-2)) is better ordered than when the target ssDNA is attached directly (Supporting Information, Fig. S1 (a)), and that probably this effect is more pronounced for longer molecules. Except for the probe DNA attachment in ss or ds form, other parameters are likely to influence the DNA orientation: the crystallinity of the diamond (the DNA may stand more or less perpendicular to the surface on a microscopic scale *i.e.* the crystal facets, but tilted to the surface plane in a more macroscopic sense), the type of linker layer (length, density, type of molecule, …),[8] the density of the DNA-layer, the length of the DNA molecules,[2] the pH and ionic strength when in buffer or the humidity of an ambient environment, the applied washing steps, and local electric fields, which can be applied to stretch DNA molecules.[3,5] Additional experiments are required to clarify the effects of these parameters. However, we are confident that the method described in this paper can be applied to test such hypotheses. Apart from fundamental research, this knowledge can be employed to understand and improve the performance of electrical hybridization measurements in a DNA sensor, such as the impedance experiments recently reported.[37]

Supporting Information Available: Further details on the diamond functionalization, SEM images of H-terminated NCD and UNCD surfaces, surface wetting experiments after various functionalization steps, fluorescence microscopy images after DNA attachment, and a further discussion of the geometrically calculated and directly measured tilt angles. This information is available free of charge via the Internet at http://pubs.acs.org.

References

[1] Moiseev, L.; Ünlü, M. S.; Swan, A. K.; Goldberg, B. B.; Cantor, C. R. *Proc. Natl. Acad. Sci. U.S.A.* **2006**, *103*, 2623.

[2] Kelley, S. O.; Barton, J. K.; Jackson, N. M.; McPherson, L. D.; Potter, A. B.; Spain, E. M.; Allen, M. J.; Hill, M. G. *Langmuir* **1998**, *14*, 6781.

[3] Zhang, Z. L.; Pang, D. W.; Zhang, R. Y. *Bioconjugate Chem.* **2002**, *13*, 104.

[4] Moses, S.; Brewer, S. H.; Lowe, L. B.; Lappi, S. E.; Gilvey, L. B.; Sauthier, M.; Tenent, R. C.; Feldheim, D. L.; Franzen, S. *Langmuir* **2004**, *20*, 11134.

[5] Anne, A.; Demaille, C. *J. Am. Chem. Soc.* **2006**, *128*, 542.

[6] Mearns, F. J.; Wong, E. L. S; Short, K.; Hibbert, D. B.; Gooding, J. J. *Electroanalyst* **2006**, *18*, 1971.

[7] Opdahl, A.; Petrovykh, D. Y.; Kimura-Suda, H.; Tarlov M.J.; Whitman, L. J. *Proc. Natl. Acad. Sci. U.S.A.* **2007**, *104*, 9.

[8] Wang, K.; Goyer, C.; Anne, A.; Demaille, C. *J. Phys. Chem. B* **2007**, *111*, 6051.

[9] Wilks, E.; Wilks, J. *Properties and applications of diamond*; Butterworth Heinemann: Oxford, 1991.

[10] Martin, H. B.; Argoitia, A.; Landau, U.; Anderson, A. B.; Angus, J. C. *J. Electrochem. Soc.* **1996**, *143*, L133.

[11] Williams, O. A.; Daenen, M.; D'Haen, J.; Haenen, K.; Maes, J.; Moshchalkov, V. V.; Nesládek, M.; Gruen, D. M. *Diamond Relat. Mater.* **2006**, *15*, 654.

[12] Yang, W.; Auciello, O.; Butler, J. E.; Cai, W.; Carlisle, J. A.; Gerbi, J. E.; Gruen, D. M.; Knickerbocker, T.; Lasseter, T. L.; Russell, J. N. Jr.; Smith, L. M.; Hamers, R. J. *Nature Mater.* **2002**, *1*, 253.

[13] Christiaens, P.; Vermeeren, V.; Wenmackers, S.; Daenen, M.; Haenen, K.; Nesládek, M.; vandeVen, M.; Ameloot, M.; Michiels, L.; Wagner, P. *Biosens. Bioelectron.* **2006**, *22*, 170.

[14] Nebel, C. E.; Uetsuka, H.; Rezek, B.; Shin, D.; Tokuda, N.; Nakamura, T. *Diamond Relat. Mater.* **2007**, *16*, 1648.

[15] Zhong, Y. L.; Chong, K. F.; May, P. W.; Chen, Z.-K.; Loh, K. P. *Langmuir* **2007**, *23*, 5824.

[16] Yang, W.; Butler, J. E.; Russell, J. N. Jr.; Hamers, R. J. *Analyst* **2007**, *132*, 296.

[17] Härtl, A.; Schmich, E.; Garrido, J. E.; Hernando, J.; Catharino, S. C. R.; Walter, S.; Feulner, P.; Kromka, A.; Steinmüller, D.; Stutzmann, M. *Nature Mater.* **2004**, *3*, 736.

[18] Song, K. S.; Degawa, M.; Nakamura, Y.; Kanazawa, H.; Umezawa, H.; Kawarada, H. *Jpn. J. Appl. Phys. Part 2* **2004**, *43*, L814.

[19] Hernando, J.; Pourrostami, T.; Garrido, J. A.; Williams, O. A.; Gruen, D. M.; Kromka, A.; Steinmüller, D.; Stutzmann, M. *Diamond Relat. Mater.* **2007**, *16*, 138.

[20] Mazur, A. K. *Phys. Rev. Lett.* **2007**, *98*, 218102.

[21] Wiggins, P. A.; Nelson, P. C. *Phys. Rev. E* **2006**, *73*, 031906.

[22] Du, Q.; Smith, C.; Shiffeldrim, N.; Vologodskaia, M.; Vologodskii, A *Proc. Natl. Acad. Sci. U.S.A.* **2005**, *102*, 5397.

[23] Shroff, H.; Reinhard, M.; Siu, M.; Agarwal, H.; Spakowitz, A.; Liphardt, J. *Nano Lett.* **2005**, *5*, 1509.

[24] Wiggins, P. A.; Heijden, T. V. D.; Moreno-Herrero, F.; Spakowitz, A.; Phillips, R.; Widom, J.; Dekker, C.; Nelson, P. C. *Nature Nanotechnol.* **2006**, *1*, 137.

[25] Sendner, C.; Kim, Y. W.; Rant, U.; Arinaga, K.; Tornow, M.; Netz, R. R. *phys. stat. sol. (a)* **2006**, *203*, 3476.

[26] Rant, U.; Arinaga, K.; Scherer, S.; Pringsheim, E.; Fujita, S.; Yokoyama, N.; Tornow, M.; Abstreiter, G. *Proc. Natl. Acad. Sci. U.S.A.* **2007**, *44*, 17364.

[27] Erts, D.; Polyakov, B.; Olin, H.; Tuite, E. *J. Phys. Chem. B* **2003**, *107*, 3591.

[28] Zhou, D.; Sinniah, K.; Abell, C.; Rayment, T. *Langmuir* **2002**, *18*, 8278.

[29] Ceres, D. M.; Barton, J. K. *J. Am. Chem. Soc.* **2003**, *125*, 14964.

[30] Nichols, B. M.; Butler, J. E.; Russell, J. N. Jr.; Hamers, R. J. *J. Phys. Chem. B* **2005**, *109*, 20938.

[31] Wenmackers, S.; Christiaens, P.; Deferme, W.; Daenen, M.; Haenen, K.; Nesládek, M.; Wagner, P.; Vermeeren, V.; Michiels, L.; vandeVen, M.; Ameloot, M.; Wouters, J.; Naelaerts, L.; Mekhalif, Z. *Mater. Sci. Forum* **2005**, *492-493*, 267.

[32] Rezek, B.; Shin, D.; Nakamura, T.; Nebel, C. E. *J. Am. Chem. Soc.* **2006**, *128*, 3884.

[33] Shin, D.; Rezek, B.; Tokuda, N.; Takeushi, D.; Watanabe, H.; Nakamura, T.; Yamamoto, T.; Nebel, C. E. *phys. stat. sol. (a)* **2006**, *203*, 3245.

[34] Rezek, B.; Shin, D.; Uetsuka, H.; Nebel, C. E. *phys. stat. sol. (a)* **2007**, *204*, 2888.

[35] Cai, W.; Peck, J. R.; van der Weide, D. W.; Hamers, R. J. *Biosens. Bioelectron.* **2004**, *19*, 1013.

[36] Gu, H. R.; Su, X.; Loh, K. P. *J. Phys. Chem. B* **2005**, *109*, 13611.

[37] Vermeeren, V.; Bijnens, N.; Wenmackers, S.; Daenen, M.; Haenen, K.; Williams, O. A.; Ameloot, M.; vandeVen, M.; Wagner, P.; Michiels, L. *Langmuir* **2007**, *23*, 13193.

[38] Ionov, L; Sidorenko, A; Eichhorn, K. J.; Stamm, M.; Minko. S.; Hinrichs, K. *Langmuir* **2005**, *21*, 8711.

[39] Vermeeren, V.; Wenmackers, S.; Daenen, M.; Haenen, K.; Williams, O. A.; Ameloot, M.; vandeVen, M.; Wagner, P.; L. Michiels, L. *Langmuir* **2008** (in press).

[40] Silaghi, S. D.; Friedrich, M.; Cobet, C.; Esser, N.; Braun, W.; Zahn, D. R. T. *phys. stat. sol. (b)* **2005**, *242*, 3047.

[41] Scholz, R.; Friedrich, M.; Salvan, G.; Kampen, T. U.; Zahn, D. R. T.; Frauenheim, T. *J. Phys. Cond. Matt.* **2003**, *15*, S2647.

[42] Rich, A.; Kasha, M. *J. Am. Chem. Soc.* **1960**, *82*, 6197.

[43] Fresco, J. R.; Lesk, A. M.; Gorn, R.; Doty, P. *J. Am. Chem. Soc.* **1961**, *83*, 3155.

[44] Inagaki, T.; Hamm, R. N.; Arakawa, E. T.; Painter, L. R. *J. Chem. Phys.* **1974**, *61*, 4246.

[45] Hinrichs, K.; Silaghi, S. D.; Cobet, C.; Esser, N.; Zahn, D. R. T. *phys. stat. sol. (b)* **2005**, *242*, 2681.

[46] Van Bael, M. K.; Nelis, D.; Hardy, A.; Mondelaers, D.; Van Werde, K.; D'Haen, J.; Vanhoyland, G.; Van den Rul, H.; Mullens, J.; Van Poucke, L. C.; Frederix, F.; Wouters, D. J. *Integrated Ferroelectrics* **2002**, *45*, 113.

[47] Heyns, M. M.; Bearda, T.; Cornelissen, I.; De Gendt, S.; Degraeve, R.; Groeseneken, G.; Kenens, C.; Knotter, D. M.; Loewenstein, L. M.; Mertens, P. W.; Mertens, S.; Meuris, M.; Nigam, T.; Schaekers, M.; Teerlinck, I.; Vandervorst, W.; Vos, R.; Wolke, K. *IBM Journal of Research and Development* **1999**, *43*, 339.

[48] Meuris, M.; Mertens, P. W.; Opdebeeck, A.; Schmidt, H. F.; Depas, M.; Vereecke, G.; Heyns, M. M.; Philipossian, A. *Solid State Technology* **1995**, *38*, 109.

[49] Tsai, W.; Carter, R. J.; Nohira, H.; Caymax, M.; Conard, T.; Cosnier, W.; DeGendt, S.; Heyns, M.; Petry, J.; Richard, O.; Vandervorst, W.; Young, E.; Zhao, C.; Maes, J.; Tuominen, M.; Schulte, W. H.; Garfunkel, E.; Gustafsson, T. *Microelectronic Engineering* **2003**, *65*, 259.

[50] Röseler, A. *Thin Solid Films* **1993**, *234*, 307.

[51] Röseler, A.; Korte, E. H. in Griffiths, P. R.; Chalmers, J. *Handbook of Vibrational Spectroscopy, vol. 2*; Wiley: Chichester, 2001.

[52] Azzam, R. M. A.; Bashara, N. M. *Ellipsometry and polarized light*; North Holland: Amsterdam, 1977.

[53] Johnson, R. L.; Barth, J.; Cardona, M.; Fuchs, D.; Bradshaw, A. M. *Rev. Sci. Instrum.* **1989**, *60*, 2209.

[54] Barth, J.; Johnson, R. L.; Cardona, M. in E. Palik *Handbook of Optical Constants of Solids II*; Academic: New York, 1991.

[55] Wethkamp, T.; Wilmers, K.; Esser, N.; Richter, W.; Ambacher, O.; Angerer, H.; Jungk, G.; Johnson, R. L.; Cardona, M. *Thin Solid Films* **1998**, *313-314*, 745.

[56] Lee, C.; Park, K. H.; Cho, M. *J. Chem. Phys.* **2006**, *125*, 114508.

[57] Liu H.-B.; Xiao, S.-J.; Chen, Y.-Q.; Chao, J.; Wang, J.; Wang, Y.; Pan, Y.; You, X. Z.; Gu Z.-Z. *J. Phys. Chem. B. Lett.* **2006**, *110*, 17702.

[58] Elhadj, S.; Singh, G.; Saraf, R. F. *Langmuir* **2004,** *20,* 5539.

[59] Legay, G.; Markey, L.; Meunier-Prest, R.; Finot, E. *Ultramicroscopy* **2007**, *107*, 1111.

[60] Banyay, M; Sarkar, M.; Gräslund, A. *Biophys. Chem.* **2003**, *104*, 477.

[61] Hagerman, P. J. *Ann. Rev. Biophys. Biophys. Chem.* **1988**, *17*, 265.

[62] Tinland, B.; Pluen, A.; Sturm, J.; Weill, G. *Macromolecules* **1997**, *30*, 5763.

[63] Sprecher, C. A.; Baase, W. A.; Curtis, W. *Biopolymers* **1979**, *18*, 1009.

[64] Kielbassa, C.; Roza, L.; Epe, B. *Carcinogenesis* **1997**, *18*, 811.

[65] Sinha, R. P.; Häder, D. P. *Photochem. Photobiol. Sci.* **2002**, *1*, 225.

[66] Liu, M.; Liu, G.-Y. *Langmuir* **2005**, *21*, 1972.

[67] Mills, J. B.; Vacano, E.; Hagerman, P. J. *J. Molec. Biol.* **1999**, *285*, 245.